

Control of the Temperature of a Finite Diffusive Interface Medium Using the CRONE Controller

X. Moreau, R. Abi Zeid Daou and F. Christophy

Abstract This chapter deals with the control of the temperature across a finite diffusive interface medium using the CRONE controller (French acronym: *Commande Robuste d'Ordre Non Entier*). In fact, the plant transfer function presents two special properties: a fractional integrator of order 0.5 and a delay factor of a fractional order (when controlling the temperature far from the boundary where the density of flux is applied). The novel approach of this work resides by the use of a fractional controller that would control a fractional order plant. Also note that the choice of the CRONE generation is important as this controller is developed in three generations: the first generation CRONE strategy is particularly appropriate when the desired open-loop gain crossover frequency ω_u is within a frequency range where the plant frequency response is asymptotic (this frequency band will be called a plant asymptotic-behavior band). As for the second generation, it is defined when ω_u is within a frequency range where the plant uncertainties are gain-like along with a constant phase variation. Concerning the third generation, it would be applied when both a gain and a phase variations are observed when dealing with plant's uncertainties. This generation will not be treated in this chapter due to some space constraints. Thus, this chapter will present some case scenarios which will lead to the use of the first two CRONE generations when using three different plants: the first one is constituted of iron, the second of aluminum and the third of copper with variable lengths L and several placements of the temperature sensor x . Simulation results will show the temperature variation across the diffusive interface medium in both time and frequency domains using Matlab and Simulink.

X. Moreau · F. Christophy

IMS Laboratory, Group CRONE, University of Bordeaux, Talence,
Bordeaux, France

e-mail: xavier.moreau@u-bordeaux.fr

F. Christophy

e-mail: fadi.christophy@u-bordeaux.fr

R. Abi Zeid Daou (✉)

Faculty of Public Health, Biomedical Technologies Department, Lebanese German
University, Sahel Alma, Jounieh, Lebanon

e-mail: r.abizeiddaou@lgu.edu.lb

© Springer International Publishing AG 2017

A.T. Azar et al. (eds.), *Fractional Order Control and Synchronization
of Chaotic Systems*, Studies in Computational Intelligence 688,
DOI 10.1007/978-3-319-50249-6_2

These results show how the temperature behaves at different positions for the three materials in use.

Keywords Finite diffusive interface • CRONE controller • Temperature control in homogeneous bars • Robustness • Users specifications • Gain and phase margin variation • Fractional order control

1 Introduction

The fractional calculus is a very old topic that was born following letter exchanges between L'Hopital and Leibtniz in September 30th, 1695 [15, 16]. Most of engineering domains have started the implementation of this topic either in the modelling process or in the control of their dynamic behavior [8]. Hence, the recognition of the fractional order in a system may reside in the identification of the plant transfer function or the control of a whole process using well known fractional controllers as the CRONE controller or the generalized PID controller [9, 17].

The diffusive interface medium is a fractional order system. In fact, the modelling of this medium has shown a semi integration (integration of order half) when considering the density of flux as the input of this medium and the temperature at any given point as the system output [7, 10]. Thus, we will consider in this work the temperature control of a finite diffusive interface after modelling, in previous works, the finite and the semi-infinite diffusive interface media [2, 3].

Hence, the novelty of this work resides in the deployment of a fractional order regulator in order to control a non-integer order plant. For this purpose, the CRONE controller will be used in its first two generations.

As each generation is used for a specific variation in the plant's transfer function, two case studies will be proposed in order to analyze the behavior and the robustness of the first two CRONE generations [1, 13].

However, lots of controllers were already synthesized and applied to several engineering fields and have shown great results. The controllers could be synthesized in both, time or frequency domain. For both cases, the fractional order has been applied. Interested readers can refer to the following papers [4–6] for more controller synthesis methods and applications.

This chapter will be divided as follow: in Sect. 2, the previous works concerning the modelling of the diffusive interface will be presented. The exact model will be proposed as well as the simplified one. Section 3 will present the CRONE controller along with the first two generations. The same example will be applied for both generations with three different gain margins. The main aim is to show the way to synthesis the CRONE controller as well as to compare between these generations. Section 4 will conclude the proposed work and will introduce some future work that may enrich this system.

2 Presentation of the Finite Diffusive Interface Medium

When presenting a finite diffusive interface medium, the heat transfer function is governed by three partial differential equations along with an initial condition regarding the initial time:

$$\begin{cases} \frac{\partial T(x,t)}{\partial t} = \alpha \frac{\partial^2 T(x,t)}{\partial x^2}, & x > 0, t > 0 \\ -\lambda \frac{\partial T(x,t)}{\partial x} = \varphi(t), & x = 0, t > 0 \\ -\lambda \frac{\partial T(x,t)}{\partial x} = 0, & x = L, t > 0 \\ T(x,t) = 0, & 0 \leq x < L, t = 0 \end{cases}. \quad (1)$$

As the temperature initial condition is null, the Laplace transform of the first equation of system (1) leads to a differential equation of order 2 with respect to the variable x , as shown in Eq. (2):

$$\frac{\partial^2 \bar{T}(x,s)}{\partial x^2} - \frac{s}{\alpha_d} \bar{T}(x,s) = 0 \text{ where } \bar{T}(x,s) = \mathcal{L}\{T(x,t)\}. \quad (2)$$

The solution of this equation is of the following form [7, 19]:

$$\bar{T}(x,s) = K_1(s) e^{x\sqrt{s/\alpha_d}} + K_2(s) e^{-x\sqrt{s/\alpha_d}}. \quad (3)$$

When taking into consideration the boundary conditions ($x = 0$ and $x = L$), a system of two equations with two unknown values, $K_1(s)$ and $K_2(s)$, is derived as shown in (4):

$$\begin{cases} K_1(s) - K_2(s) = -\frac{1}{\lambda\sqrt{s/\alpha_d}} \bar{\varphi}(s) \\ K_1(s) e^{L\sqrt{s/\alpha_d}} - K_2(s) e^{-L\sqrt{s/\alpha_d}} = 0 \end{cases}. \quad (4)$$

The solution of this system, after the introduction of a new parameter $\lambda = \alpha_d \rho C_p$, leads to the expressions of $K_1(s)$ and $K_2(s)$, as shown below:

$$\begin{cases} K_1(s) = \frac{1}{\sqrt{\lambda \rho C_p s}} \frac{e^{-L\sqrt{s/\alpha_d}}}{e^{L\sqrt{s/\alpha_d}} - e^{-L\sqrt{s/\alpha_d}}} \bar{\varphi}(s) \\ K_2(s) = \frac{1}{\sqrt{\lambda \rho C_p s}} \frac{e^{L\sqrt{s/\alpha_d}}}{e^{L\sqrt{s/\alpha_d}} - e^{-L\sqrt{s/\alpha_d}}} \bar{\varphi}(s) \end{cases}. \quad (5)$$

The introduction of system Eq. (5) in Eq. (3) and the replacement of the flux density $\bar{\varphi}(s)$ by the flux $\bar{\Phi}(s)$ ($\bar{\varphi}(s) = \bar{\Phi}(s)/S$) lead to the below transfer function of the whole system:

$$H(x, s, L) = \frac{\bar{T}(x, s, L)}{\bar{\phi}(s)} = \frac{1}{S\sqrt{\lambda\rho}C_p s} \frac{e^{-(L-x)\sqrt{s/\alpha_d}} + e^{(L-x)\sqrt{s/\alpha_d}}}{e^{L\sqrt{s/\alpha_d}} - e^{-L\sqrt{s/\alpha_d}}}, \quad (6)$$

which can be also presented as follow after introducing the hyperbolic functions [3]

$$H(x, s, L) = \frac{\bar{T}(x, s, L)}{\bar{\phi}(s)} = \frac{1}{S\sqrt{\lambda\rho}C_p s} \frac{1}{\tanh\left(L\sqrt{\frac{s}{\alpha_d}}\right)} \frac{\cosh\left((L-x)\sqrt{\frac{s}{\alpha_d}}\right)}{\cosh\left(L\sqrt{\frac{s}{\alpha_d}}\right)}. \quad (7)$$

Hence, to sum up, the system transfer function can be partitioned in several blocks as shown in Fig. 1 and as mentioned in systems (8)–(10).

$$H(x, s, L) = H_0 I^{0.5}(s) F(0, s, L) G(x, s, L), \quad (8)$$

where

$$\begin{cases} H_0 = \frac{s^{0.5} \bar{T}(0, s, \infty)}{\bar{\phi}(s)} = \frac{1}{S\eta_d} \\ I^{0.5}(s) = \frac{\bar{T}(0, s, \infty)}{s^{0.5} \bar{T}(0, s, \infty)} = \frac{1}{s^{0.5}} \\ F(0, s, L) = \frac{\bar{T}(0, s, L)}{\bar{T}(0, s, \infty)} = \frac{1}{\tanh\left(\sqrt{\frac{s}{\omega_L}}\right)}, \\ G(x, s, L) = \frac{\bar{T}(x, s, L)}{\bar{T}(0, s, L)} = \frac{\cosh\left(\sqrt{\frac{s}{\omega_{Lx}}}\right)}{\cosh\left(\sqrt{\frac{s}{\omega_L}}\right)} \end{cases} \quad (9)$$

knowing that

$$\begin{cases} \eta_d = \sqrt{\lambda\rho C_p} \\ \omega_L = \frac{\alpha_d}{L^2} \\ \omega_{Lx} = \frac{\alpha_d}{(L-x)^2} \end{cases}, \quad (10)$$

where η_d represents the thermal effusivity.

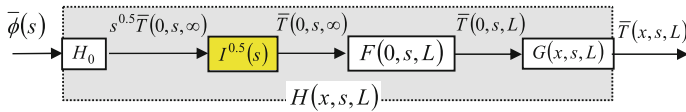


Fig. 1 Block diagram of the finite medium transfer function

Table 1 Physical characteristics of the used materials

Material	α_d m ² /s	η_d W.K ⁻¹ .m ⁻² .s ^{0.5}	H_o K.s ^{0.5} .W ⁻¹	ω_L (rad/s)			ω_x (rad/s)		
				L = 0.25 m	L = 0.5 m	L = 1 m	x = 0	x = 0.5 cm	x = 1 cm
Copper	117 × 10 ⁻⁶	3.72 × 10 ⁴	0.269	19 × 10 ⁻⁴	4.68 × 10 ⁻⁴	1.17 × 10 ⁻⁴	Inf.	4.68	1.17
Aluminium	97 × 10 ⁻⁶	2.41 × 10 ⁴	0.416	16 × 10 ⁻⁴	3.88 × 10 ⁻⁴	0.97 × 10 ⁻⁴	Inf.	3.88	0.97
Iron	23 × 10 ⁻⁶	1.67 × 10 ⁴	0.596	3.68 × 10 ⁻⁴	0.92 × 10 ⁻⁴	0.23 × 10 ⁻⁴	Inf.	0.92	0.23

Note that, for analysis purposes, a relation between ω_L , ω_{Lx} and the diffusive time constant, τ_L , were introduced:

$$\begin{cases} \omega_L = \left(1 - \frac{x}{L}\right)^2 \omega_{Lx} \\ \tau_L = \frac{1}{\omega_L} = \frac{L^2}{\alpha_d} \end{cases} \quad (11)$$

The approximation of this system was already presented in several previous works. Interested authors can refer to the following references [3, 10, 12]. Just need to know that Oustaloup approximation and Maclaurin series were at the core of this approximation. As a conclusion, the finite diffusive interface medium can be approximated by the following transfer function:

$$H(x, s, L) = \frac{\bar{T}(x, s, L)}{\bar{\phi}(s)} = H_0 \frac{1}{s^{0.5}} \frac{1}{\tanh\left(\sqrt{\frac{s}{\omega_L}}\right)} e^{-\sqrt{\frac{s}{\omega_x}}}, \quad (12)$$

where $\omega_x = \alpha_d/x^2$.

At the end of this section, let us define the different materials to be used for the control process. In fact, the aluminum, the copper and the iron were used for the simulations later in this chapter. All physical values of these three materials will be presented in Table 1.

3 CRONE Controller

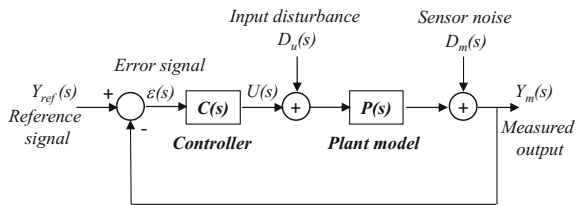
CRONE is the acronym for *Commande Robuste d'Ordre Non Entier* (non-integer order robust control). While the first two approaches use the real fractional integration or differentiation operator, the third uses the complex differentiation operator. In the frequency domain, they enable to synthesize simply and methodologically, linear robust control laws. The control schematic used is based on the classic unity-feedback configuration. Thus, Fig. 2 shows a general scheme used for the control-system design.

The equations associated to this scheme are given by:

- Output: $Y(s) = S(s) D_m(s) + SP(s) D_u(s) + T(s) Y_{ref}(s)$ (13)

- Error signal: $\varepsilon(s) = -S(s) D_m(s) - SP(s) D_u(s) + S(s) Y_{ref}(s)$ (14)

Fig. 2 Scheme used for the control-system design



- Controlsignal: $U(s) = -SC(s) D_m(s) + T(s) D_u(s) + SC(s) Y_{ref}(s)$ (15)

with

$$\begin{cases} S(s) = \frac{1}{1+\beta(s)}: & \text{sensitivity function} \\ T(s) = 1 - S(s): & \text{complementary sensitivity function} \\ SP(s) = S(s) P(s) \\ SC(s) = S(s) C(s) \\ \beta(s) = C(s) G(s): & \text{open-loop transfer function} \end{cases} \quad (16)$$

As the main purpose is not to present the CRONE controller but to provide the tools used to fit the user specifications concerning the stability degree, the rapidity, the precision in the steady state mode, the saturation as well as the sensibility of the system towards the disturbances, we will present hereafter the general transfer functions of the first two CRONE generations along with the conditions that must be filled in order to apply each of these generations.

The user specifications lead us to set the following parameters:

- Concerning the **stability degree**, the phase margin M_ϕ varies between $90^\circ \geq M_\phi \geq 45^\circ$;
- Concerning the **speed**, desired open-loop gain crossover frequency ω_u (or ω_{cg}) is equal to 1 rad/s;
- Concerning the **precision in the steady state response**, a null static error;
- Concerning the **saturation**, a maximum input value of 12 W is allowed.

3.1 Synthesis with Gain Variations Only

In this first part, we will treat the gain variations only while considering a constant phase. Thus, the first CRONE generation could be used as well as the second one.

3.1.1 First Generation CRONE Controller

The transfer function of the synthesized model of the plant that would be used for the control purposes at the boundary where the flux is applied (e.g., for $x = 0$ mm) is Poinot and Trigeassou [18], Malti et al. [14]:

$$P_1(s) = H(0, s, L) = H_0 \frac{1}{s^{0.5}} \frac{1}{\tanh\left(\sqrt{\frac{s}{\omega_L}}\right)}, \quad (17)$$

where the nominal state parameters (for the aluminum case) are:

$$\begin{cases} H_0 = H_0(\text{Alu}) = 0.416 \text{ K s}^{0.5} \text{ W}^{-1} \\ \omega_L = \omega_L(\text{Alu}, L = 1\text{ m}) = 0.97 \cdot 10^{-4} \text{ rad/s} \end{cases}, \quad (18)$$

and their variation ranges taking into account the two other materials already shown in Table 1:

$$\begin{cases} H_0 \in [\underline{H_0} = H_0(\text{Cop}) = 0.269 \quad ; \quad \overline{H_0} = H_0(\text{Iron}) = 0.596] \text{ K s}^{0.5} \text{ W}^{-1} \\ \omega_L \in [\underline{\omega_L} = \omega_L(\text{Iron}, L = 1 \text{ m}) = 0.23 \cdot 10^{-4} \text{ rad/s} \quad ; \quad \overline{\omega_L} = \omega_L(\text{Cop}, L = 0.25 \text{ m}) = 19 \cdot 10^{-4} \text{ rad/s}] \end{cases} \quad (19)$$

As for the first generation CRONE controller, its transfer function is of the following form [11]:

$$C_F(s) = C_0 \left(\frac{1 + s/\omega_l}{s/\omega_l} \right)^{m_l} \left(\frac{1 + s/\omega_l}{1 + s/\omega_h} \right)^m \frac{1}{(1 + s/\omega_F)^{m_F}}, \quad (20)$$

where $m_l, m_F \in \mathbf{N}$, $\omega_l < \omega_F \in \mathbb{R}$ and $\omega_l < \omega_h \in \mathbb{R}$.

If we choose $\omega_l = \omega_l$ and $\omega_h = \omega_F$ in order to simplify the transfer function of the controller while taking into consideration the user specifications already defined at the beginning of this section, we can get:

$$C_F(s) = C_0 \left(\frac{\omega_l}{s} \right)^{m_l} \frac{(1 + s/\omega_l)^{m_l + m}}{(1 + s/\omega_h)^{m_F + m}}. \quad (21)$$

Referring to the synthesis characteristics, we choose:

- $m_l = 1$, in order to get a null static error as the plant contains an integration of order 1 at low frequencies;
- $m = (M_\phi - 180^\circ - \arg P_1(j\omega_u)) / 90^\circ$, which is based on the definition of the phase margin M_ϕ , knowing that $\arg P_1(j\omega_u) = -45^\circ$, thus $M_\phi \in [45^\circ; 90^\circ]$, hence $m \in [-1; -0.5]$;
- $m_F = 1$, in order to limit the input sensitivity;
- $\omega_{unom} = 1 \text{ rad/s}$, value defined by the authors;

Based on these values, the expression of $C_F(s)$ can be rewritten as follow:

$$C_F(s) = C_0 \left(\frac{\omega_l}{s} \right) \left(\frac{1 + s/\omega_l}{1 + s/\omega_h} \right)^{1+m}. \quad (22)$$

Thus, knowing that $m \in [-1; -0.5]$ and $\omega_l < \omega_h$, the fractional form of the controller $C_F(s)$ can be expressed by an integrator of order 1 in series with a lead compensator of order $1 + m$, m being a non-integer value. The expression of $C_F(s)$ is thus characterized by four parameters (m , ω_l , ω_h et C_0) that could be defined based on three below steps:

Step 1 m is determined based on the phase margin M_ϕ ;

Step 2 ω_l and ω_h are defined in such a way that the fractional asymptotic behavior of the controller should vary in a frequency range between $[\omega_A, \omega_B]$ around the nominal gain cutoff frequency ω_{unom} . In order to keep the stability degree robustness, it is necessary to set the following:

$$\forall \omega_u \in [\omega_{u \min}; \omega_{u \max}], \omega_A \leq \omega_u \leq \omega_B \Rightarrow \begin{cases} \omega_A \leq \omega_{u \min} \\ \omega_B \geq \omega_{u \max} \end{cases}, \quad (23)$$

and

$$\begin{cases} \omega_l = \omega_A / b \\ \omega_h = b \omega_B \end{cases}, \quad \text{where } b > 1. \quad (24)$$

If we consider that ω_l and ω_h are geometrically distributed around the cutoff frequency ω_{unom} and if we suppose that $r = \omega_B / \omega_A$, ω_l and ω_h would be calculated as follow:

$$\begin{cases} \sqrt{\omega_l \omega_h} = \omega_{unom} \\ \frac{\omega_h}{\omega_l} = b^2 r \end{cases} \Rightarrow \begin{cases} \omega_l = \omega_{unom} / (b \sqrt{r}) \\ \omega_h = \omega_{unom} b \sqrt{r} \end{cases}. \quad (25)$$

The value of the ratio r is deduced from the slope $-n20$ dB/dec (n being defined based on the open loop transfer function order around ω_{unom}) and from the gain variation $\Delta\beta$ due to the parametric uncertainties, thus:

$$r = \Delta\beta^{1/n}. \quad (26)$$

Step 3 C_0 is calculated in order to respond to the speed specifications. Hence, C_0 can be calculated based on the following relation:

$$|\beta(j\omega_u)| = 1 \Leftrightarrow |C_F(j\omega_u)| |P_1(j\omega_u)| = 1, \quad (27)$$

which can be also expressed as follows:

$$C_0 \left(\frac{\omega_l}{\omega_u} \right) \left(\frac{1 + (\omega_u/\omega_l)^2}{1 + (\omega_u/\omega_h)^2} \right)^{\left(\frac{1+m}{2}\right)} |P_1(j\omega_u)| = 1, \quad (28)$$

thus,

$$C_0 = \left[\left(\frac{\omega_l}{\omega_u} \right) \left(\frac{1 + (\omega_u/\omega_l)^2}{1 + (\omega_u/\omega_h)^2} \right)^{\left(\frac{1+m}{2}\right)} |P_1(j\omega_u)| \right]^{-1}. \quad (29)$$

Finally, the last step consists on presenting the controller fractional order transfer function $C_F(s)$ in a rational form $C_R(s)$. Different approaches were proposed but Oustaloup approximation remains one of the best. Hence, applying it will lead to the following general form of the controller:

$$C_R(s) = C_0 \left(\frac{\omega_l}{s} \right) \prod_{i=1}^N \left(\frac{1 + s/\omega_i'}{1 + s/\omega_i} \right), \quad (30)$$

where

$$\begin{cases} \frac{\omega_{i+1}'}{\omega_i} = \frac{\omega_{i+1}}{\omega_i} = \alpha\eta > 1 \\ \frac{\omega_i}{\omega_i} = \alpha \text{ et } \frac{\omega_{i+1}'}{\omega_i} = \eta \\ \alpha\eta = (\omega_h/\omega_l)^{1/N} \\ \alpha = (\alpha\eta)^{1+m} \text{ et } \eta = (\alpha\eta)^{-m} \\ \omega_1' = \omega_1\eta^{1/2} \text{ et } \omega_N = \omega_h\eta^{-1/2} \end{cases}. \quad (31)$$

The remaining part of this paragraph will show the 1st generation CRONE controller computation for three phase margin values $M_\phi = 45^\circ$, 67.5° and 90° and its robustness when applying it to the three materials (aluminum, copper and iron).

Example 1: Phase Margin $M_\phi = 45^\circ$

If $M_\phi = 45^\circ$, then $m = (M_\phi - 180^\circ - \arg P_1(j\omega_u))/90^\circ = -1$. The controller transfer function can be expressed as shown in Eq. (32):

$$C_F(s) = C_0 \left(\frac{\omega_l}{s} \right). \quad (32)$$

This is a particular case as the controller is expressed as an integrator of order 1 characterized by only one parameter $C_0^* = C_0 \omega_l$ whose main purpose is to take in consideration the speed specification, thus:

$$|\beta(j\omega_u)| = 1 \Leftrightarrow |C_F(j\omega_u)| |P_1(j\omega_u)| = 1, \quad (33)$$

which can also be expressed as follow:

$$\frac{C_0^*}{\omega_u} |P_1(j\omega_u)| = 1, \quad (34)$$

thus,

$$C_0^* = \frac{\omega_u}{|P_1(j\omega_u)|} \Rightarrow C_0^* = 2.405 V/^\circ. \quad (35)$$

As the controller is of an integer form in this case, the transfer functions of $C_F(s)$ and $C_R(s)$ are similar.

Example 2: Phase Margin $M_\phi = 67.5^\circ$

If $M_\phi = 67.5^\circ$, then $m = (M_\phi - 180^\circ - \arg P_1(j\omega_u)) / 90^\circ = -0.75$. The controller transfer function can be expressed as shown in Eq. (36):

$$C_F(s) = C_0 \left(\frac{\omega_l}{s} \right) \left(\frac{1 + s/\omega_l}{1 + s/\omega_h} \right)^{0.25}. \quad (36)$$

In this second example, the controller could be expressed as an integrator of order 1 in series with a lead compensator of order 0.25. The gain C_0 and the open-loop gain crossover frequency are defined as follow:

$$\left\{ \begin{array}{l} \omega_A = \omega_{u \min} = 72.77 \cdot 10^{-2} \text{ rad/s} \\ \omega_B = \omega_{u \max} = 137.43 \cdot 10^{-2} \text{ rad/s} \end{array} \right\} \Rightarrow r = 1.89$$

$$\left\{ \begin{array}{l} b = 25 \\ C_0 = 34.125 \text{ V } s/^\circ \end{array} \right\} \Rightarrow \left\{ \begin{array}{l} \omega_l = 2.91 \cdot 10^{-2} \text{ rad/s} \\ \omega_h = 34.36 \text{ rad/s} \end{array} \right. . \quad (37)$$

The rational form of this controller (who is expressed in Eq. (30)) will have the below values:

$$\left\{ \begin{array}{ll} N=6 \\ \omega'_1 = 8.17 \cdot 10^{-2} \text{ rad/s} & \omega_1 = 3.37 \cdot 10^{-2} \text{ rad/s} \\ \omega'_2 = 26.55 \cdot 10^{-2} \text{ rad/s} & \omega_2 = 10.96 \cdot 10^{-2} \text{ rad/s} \\ \omega'_3 = 86.3 \cdot 10^{-2} \text{ rad/s} & \omega_3 = 35.64 \cdot 10^{-2} \text{ rad/s} . \\ \omega'_4 = 2.81 \text{ rad/s} & \omega_4 = 1.159 \text{ rad/s} \\ \omega'_5 = 9.12 \text{ rad/s} & \omega_6 = 3.77 \text{ rad/s} \\ \omega'_6 = 29.65 \text{ rad/s} & \omega_7 = 12.25 \text{ rad/s} \end{array} \right. \quad (38)$$

Example 3: Phase Margin $M_\Phi = 90^\circ$

If $M_\Phi = 90^\circ$, then $m = (M_\Phi - 180^\circ - \arg P_1(j\omega_u)) / 90^\circ = -0.5$. The controller transfer function can be expressed as shown in Eq. (39):

$$C_F(s) = C_0 \left(\frac{\omega_l}{s} \right) \left(\frac{1 + s/\omega_l}{1 + s/\omega_h} \right)^{0.5}. \quad (39)$$

In this example, the controller could be expressed as an integrator of order 1 in series with a lead compensator of order 0.5. The gain C_0 and the open-loop gain crossover frequency are defined based on system (40):

$$\left\{ \begin{array}{l} \omega_A = \omega_{u \min} = 67.21 \cdot 10^{-2} \text{ rad/s} \\ \omega_B = \omega_{u \max} = 148.8 \cdot 10^{-2} \text{ rad/s} \end{array} \right\} \Rightarrow r = 2.214$$

$$\left\{ \begin{array}{l} b = 25 \Rightarrow \left\{ \begin{array}{l} \omega_l = 2.69 \cdot 10^{-2} \text{ rad/s} \\ \omega_h = 37.2 \text{ rad/s} \end{array} \right. \\ C_0 = 14.67 \text{ V s/}^\circ \end{array} \right. , \quad (40)$$

As for the parameters of the rational transfer function $C_R(s)$, they are as follow:

$$\left\{ \begin{array}{ll} N=6 \\ \omega'_1 = 6.64 \cdot 10^{-2} \text{ rad/s} & \omega_1 = 3.63 \cdot 10^{-2} \text{ rad/s} \\ \omega'_2 = 22.16 \cdot 10^{-2} \text{ rad/s} & \omega_2 = 12.13 \cdot 10^{-2} \text{ rad/s} \\ \omega'_3 = 73.98 \cdot 10^{-2} \text{ rad/s} & \omega_3 = 40.49 \cdot 10^{-2} \text{ rad/s} . \\ \omega'_4 = 2.47 \text{ rad/s} & \omega_4 = 1.352 \text{ rad/s} \\ \omega'_5 = 8.24 \text{ rad/s} & \omega_6 = 4.51 \text{ rad/s} \\ \omega'_6 = 27.52 \text{ rad/s} & \omega_7 = 15.06 \text{ rad/s} \end{array} \right. \quad (41)$$

Performances

Figures 3, 4, 5, 6, 7, 8 show the frequency domain and time domain performances for the three examples when applying the three different materials. In fact, Fig. 3 shows the Bode diagrams of $C_F(s)$ for the three listed examples ($M_\Phi = 45^\circ$ (a), $M_\Phi = 67.5^\circ$ (b) and $M_\Phi = 90^\circ$ (c)).

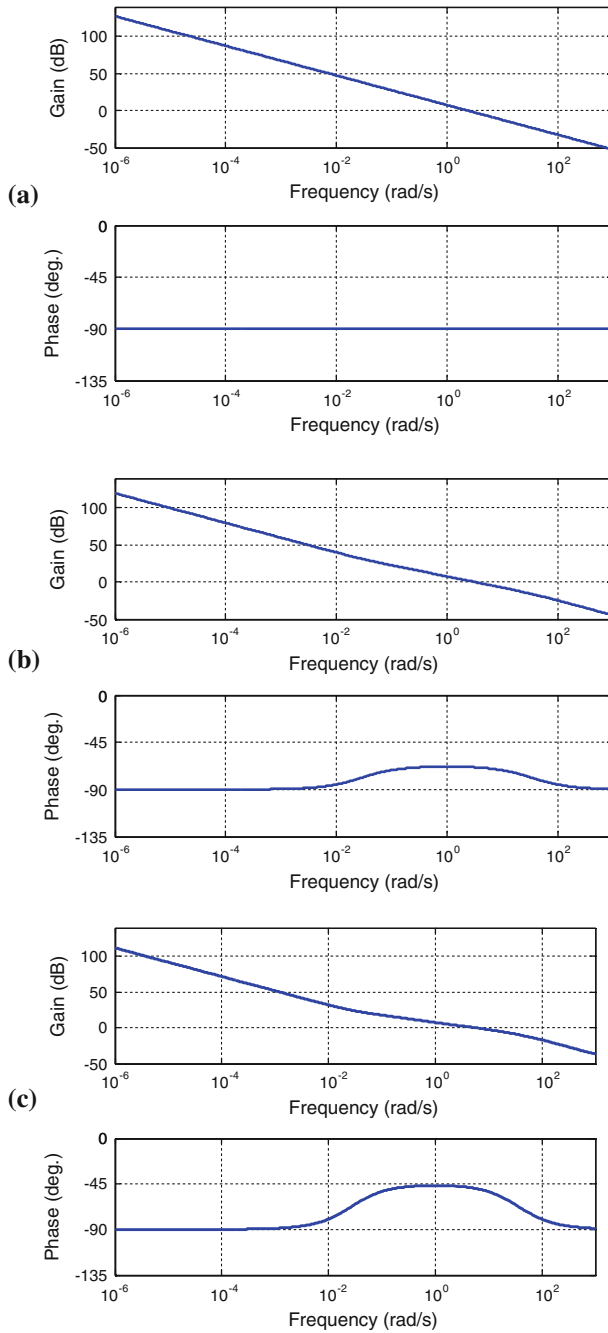


Fig. 3 Bode diagrams for CRONE controller $C_F(s)$ for $M_\Phi = 45^\circ$ (a), $M_\Phi = 67.5^\circ$ (b) and $M_\Phi = 90^\circ$ (c)

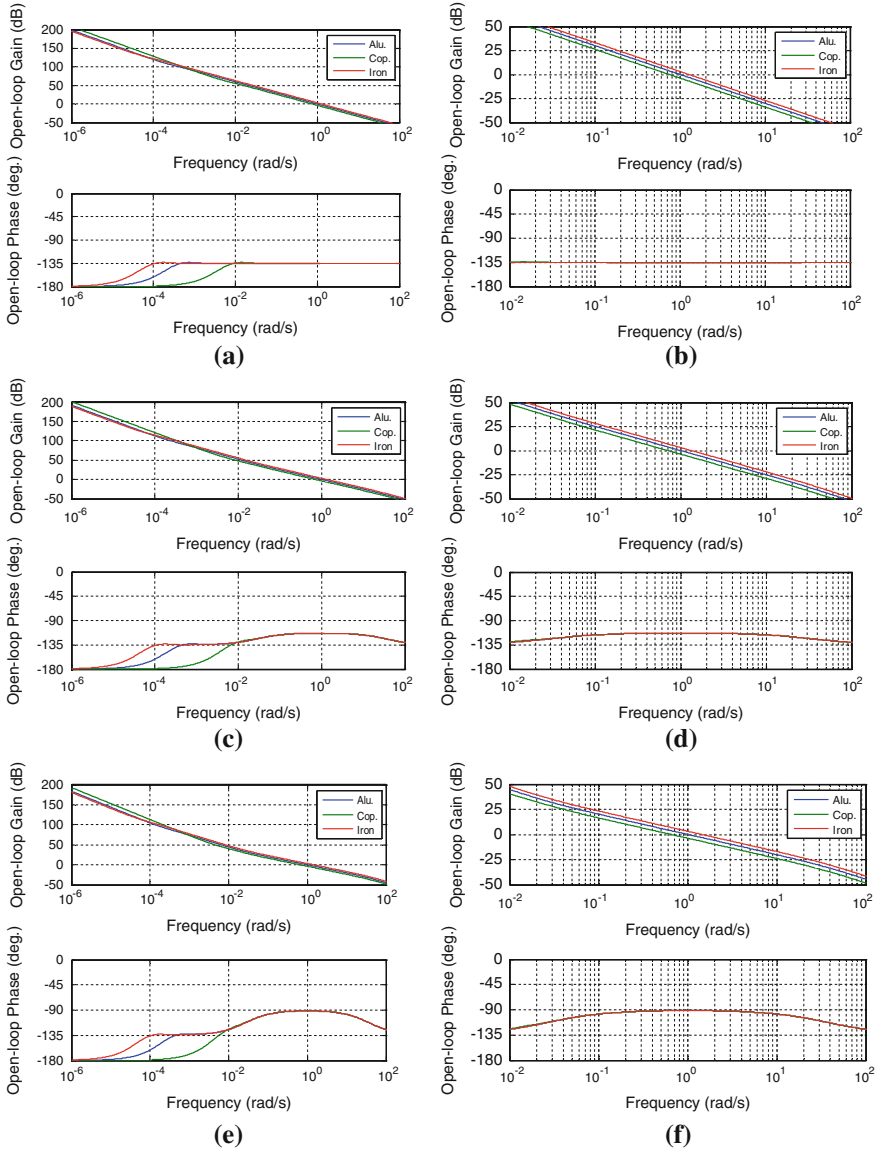


Fig. 4 Bode diagrams for the open loop transfer function over the interval $[10^{-6}$ rad/s; 10 rad/s] (a, c, e), and with a zoom around the gain crossover frequency $\omega_u = 1$ rad/s (b, d, f), for $M_\phi = 45^\circ$ (a, b), $M_\phi = 67.5^\circ$ (c, d) and $M_\phi = 90^\circ$ (e, f)

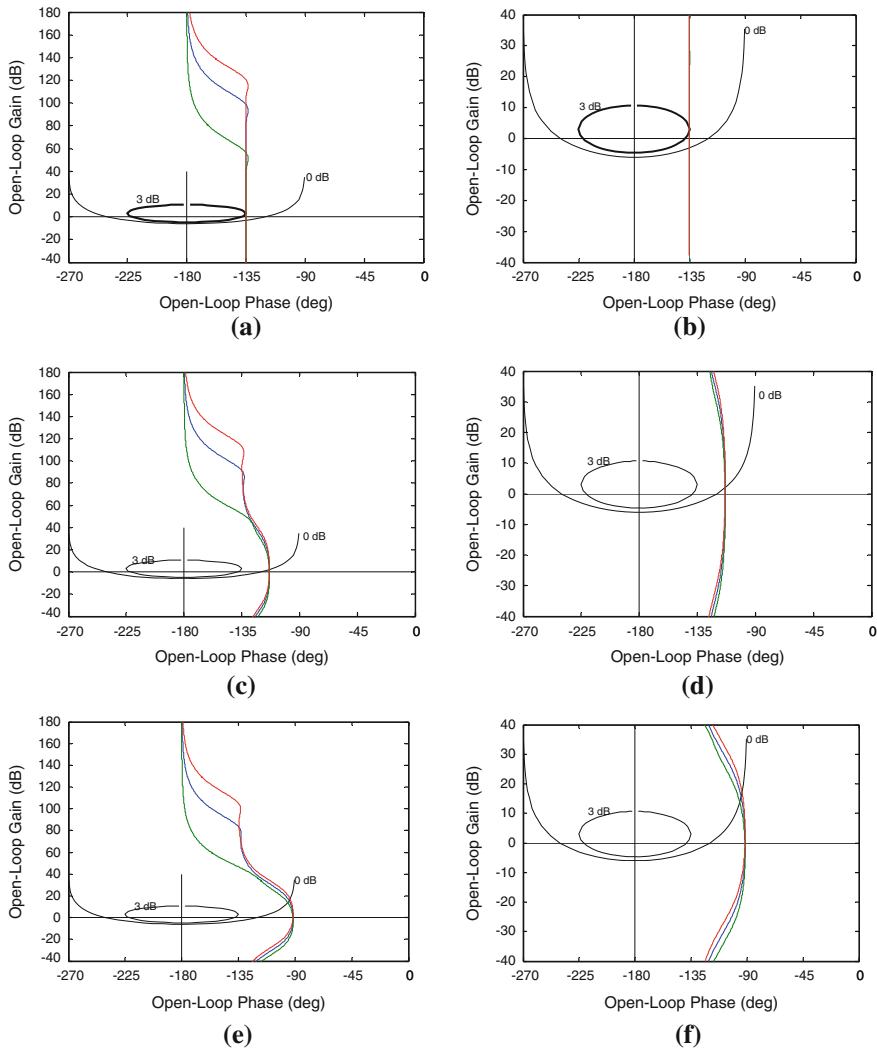


Fig. 5 Black-Nichols plots for the open loop transfer function over the interval $[-40 \text{ dB}; 180 \text{ dB}]$ (a, c, e) and with a zoom around the gain crossover frequency $\omega_u = 1 \text{ rad/s}$ (b, d, f), for $M_\phi = 45^\circ$ (a, b), $M_\phi = 67.5^\circ$ (c, d) and $M_\phi = 90^\circ$ (e, f)

Figure 4 shows the open loop Bode diagrams over the frequency bandwidth $[10^{-6} \text{ rad/s}; 10 \text{ rad/s}]$ in (a) (c) (e), with a particular zoom around the open-loop gain crossover frequency $\omega_u = 1 \text{ rad/s}$ in (b) (d) (f), for $M_\phi = 45^\circ$ (a) (b), $M_\phi = 67.5^\circ$ (c) (d) and $M_\phi = 90^\circ$ (e) (f).

Figure 5 presents the Black-Nichols plots of the open loop transfer function over the interval $[-40 \text{ dB}; 180 \text{ dB}]$ in (a) (c) (e) with a particular zoom around the

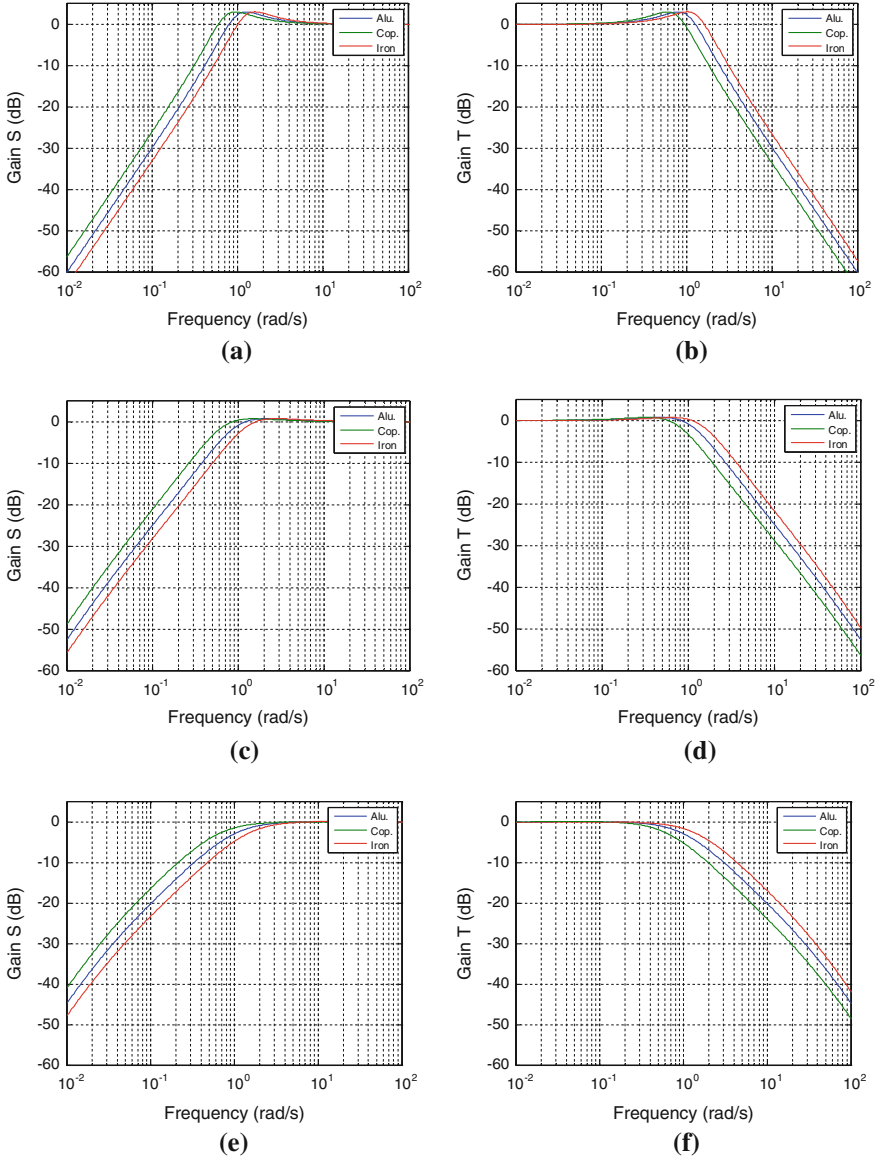


Fig. 6 Gain diagrams for the sensitivity functions: $S(j\omega)$ (a, c, e) and $T(j\omega)$ (b, d, f), for $M_\phi = 45^\circ$ (a, b), $M_\phi = 67.5^\circ$ (c, d) and $M_\phi = 90^\circ$ (e, f)

open-loop gain crossover frequency $\omega_u = 1$ rad/s in (b) (d) (f), for $M_\phi = 45^\circ$ (a) (b), $M_\phi = 67.5^\circ$ (c) (d) and $M_\phi = 90^\circ$ (e) (f).

Figure 6 shows the gain diagrams for the sensitivity functions $S(j\omega)$ in (a) (c) (e) and $T(j\omega)$ in (b) (d) (f), for $M_\phi = 45^\circ$ (a) (b), $M_\phi = 67.5^\circ$ (c) (d) and $M_\phi = 90^\circ$ (e) (f).

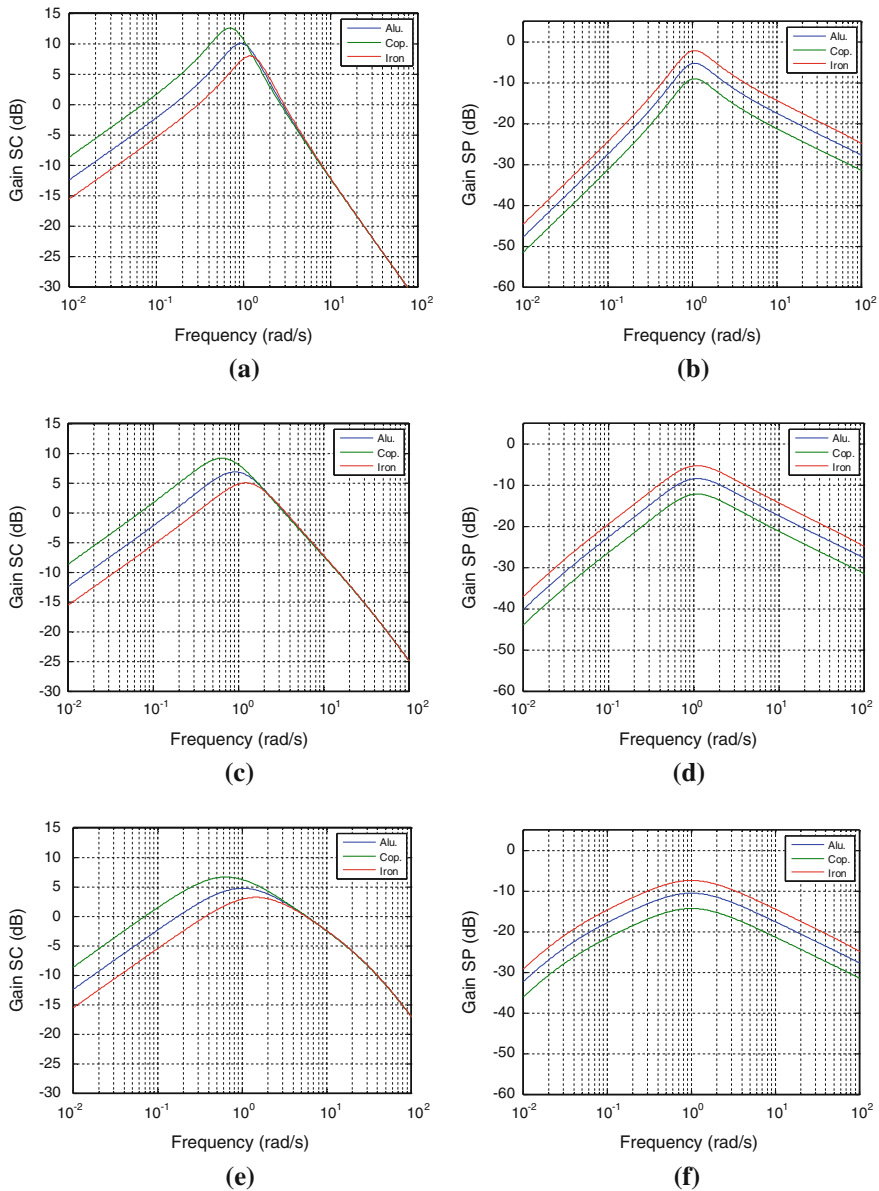


Fig. 7 Gain diagrams for the sensitivity functions: $SC(j\omega)$ (a, c, e) and $SP(j\omega)$ (b, d, f), for $M_\phi = 45^\circ$ (a, b), $M_\phi = 67.5^\circ$ (c, d) and $M_\phi = 90^\circ$ (e, f)

Figure 7 presents the gain diagrams of the sensitivity functions $SC(j\omega)$ in (a) (c) (e) et $SP(j\omega)$ in (b) (d) (f), for $M_\phi = 45^\circ$ (a) (b), $M_\phi = 67.5^\circ$ (c) (d) and $M_\phi = 90^\circ$ (e) (f).

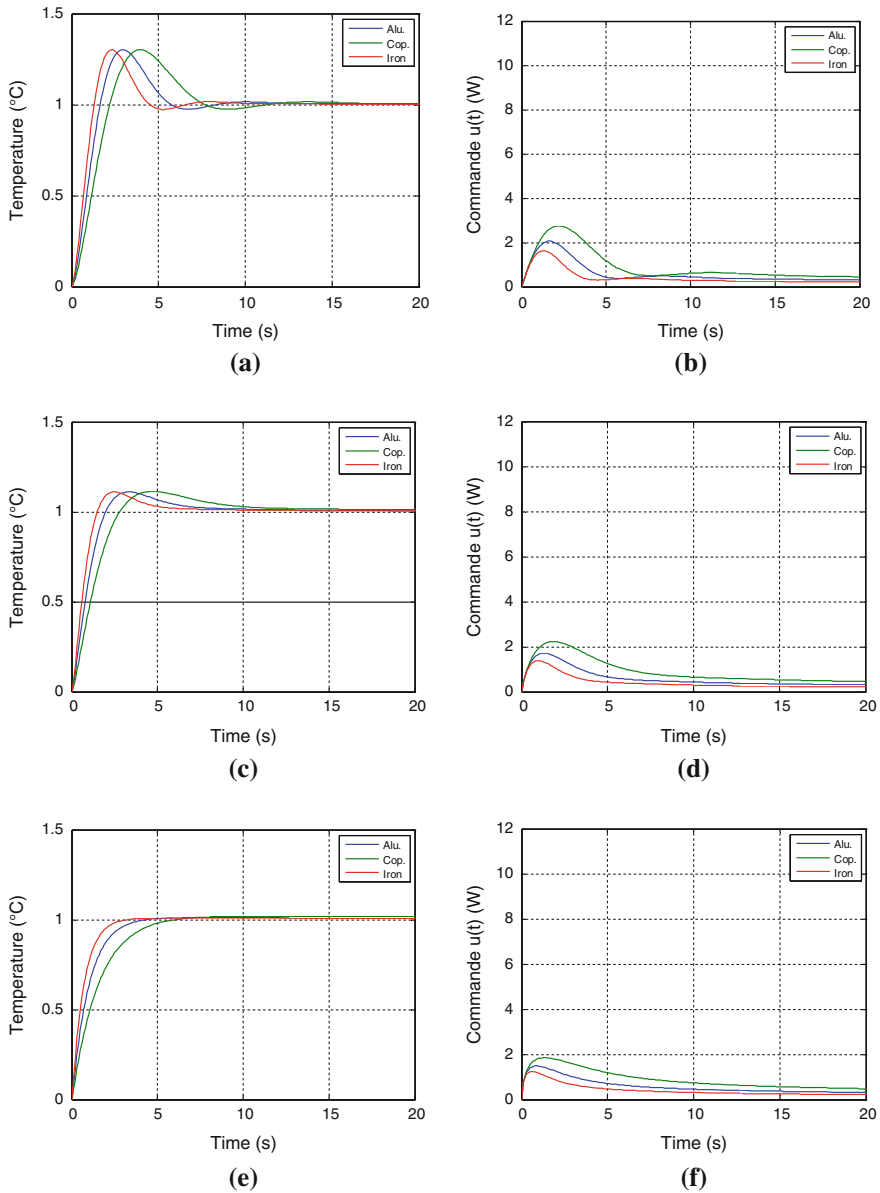


Fig. 8 Time domain responses for a step input of 1 °C: output temperature (a, c, e) and control signal (b, d, f), for $M_\phi = 45^\circ$ (a, b), $M_\phi = 67.5^\circ$ (c, d) and $M_\phi = 90^\circ$ (e, f)

Finally, Fig. 8 shows the output temperature variations for step input of amplitude 1 °C in (a) (c) (e) and for the control signal in (b) (d) (f), for $M_\phi = 45^\circ$ (a) (b), $M_\phi = 67.5^\circ$ (c) (d) and $M_\phi = 90^\circ$ (e) (f).

The robustness study is also presented in these figures as the plots contain the behavior of the three different materials.

3.1.2 Second Generation CRONE Controller

Let's start by a review of the plant simplified transfer function. In fact, the model $P_{2.1}(s)$ will be used to synthesize the second generation CRONE controller. Its transfer function is as follow:

$$P_{2.1}(s) = H_0^* \frac{(1 + s/\omega_L)^{0.5}}{s/\omega_L}, \quad (42)$$

where

$$H_0^* = \frac{H_0}{\omega_L^{0.5}}, \quad (43)$$

and where the values of the variables H_0 and ω_L were already presented in Eq. (14) along with their intervals (system (19)).

As for the CRONE controller synthesis, it is done a posteriori when applying the second generation. Hence, the open loop transfer function is expressed as follow:

$$\beta(s) = \beta_0 \left(\frac{1 + s/\omega_l}{s/\omega_l} \right)^{n_l} \left(\frac{1 + s/\omega_h}{1 + s/\omega_l} \right)^n \frac{1}{(1 + s/\omega_h)^{n_h}}, \quad (44)$$

where ω_l and ω_h represent the transitional low and high frequencies, n a real non-integer order between 1 and 2 near the frequency ω_u , n_l and n_h are the orders of the asymptotic behavior at low and high frequencies and β_0 a constant which ensures unity gain at frequency ω_u .

Thus, after defining the open loop transfer function, the computation of the fractional order CRONE controller is defined as follow:

$$C_F(s) = \beta(s) P_{2.1}^{-1}(s). \quad (45)$$

Hence, $C_F(s)$ could be written as follow:

$$C_F(s) = \beta_0 \left(\frac{1 + s/\omega_l}{s/\omega_l} \right)^{n_l} \left(\frac{1 + s/\omega_h}{1 + s/\omega_l} \right)^n \frac{1}{(1 + s/\omega_h)^{n_h}} \frac{s/\omega_L}{H_0^* (1 + s/\omega_L)^{0.5}}. \quad (46)$$

Referring to the user specifications already shown at the start of this section, the parameters values of Eq. (46) are set as follow:

- $n_l = 2$, in order to get a null static error;

- $n = (180^\circ - M_\phi)/90^\circ$, in order to have a phase margin $M_\phi \in [45^\circ; 90^\circ]$; thus $n \in [1; 1.5]$;
- $n_h = 1.5$, in order to limit the input sensitivity;
- $\omega_{unom} = 1$ rad/s, value defined by the user and applied for all examples for a comparative study.

Hence, expression (46) can be rewritten as follow:

$$C_F(s) = C_0 \left(\frac{\omega_l}{s} \right) \left(\frac{1 + s/\omega_l}{1 + s/\omega_h} \right)^{2-n} \left(\frac{1 + s/\omega_h}{1 + s/\omega_L} \right)^{0.5}, \quad (47)$$

where

$$C_0 = \frac{\beta_0 \omega_l}{H_0^* \omega_L}. \quad (48)$$

As for the first generation, this paragraph will also study the system behavior while applying the second generation CRONE controller for three different cases when the phase margin M_ϕ is equal to 45° , 67.5° and 90° .

Example 4: Phase Margin $M_\phi = 45^\circ$

If $M_\phi = 45^\circ$, then $n = (180^\circ - M_\phi)/90^\circ = 1.5$. The open loop transfer function can be expressed as follow:

$$\beta(s) = \beta_0 \frac{(1 + s/\omega_l)^{0.5}}{(s/\omega_l)^2}, \quad (49)$$

and the controller transfer function would be:

$$C_F(s) = C_0 \left(\frac{\omega_l}{s} \right) \left(\frac{1 + s/\omega_l}{1 + s/\omega_L} \right)^{0.5}. \quad (50)$$

If we suppose that $\omega_l = \omega_L$, $C_F(s)$ can be rewritten as shown in Eq. (51):

$$C_F(s) = C_0 \left(\frac{\omega_l}{s} \right). \quad (51)$$

This expression is identical to the one of the first generation CRONE controller obtained in example 1 of Sect. 3.1.1.

Example 5: Phase Margin $M_\phi = 67.5^\circ$

If $M_\phi = 67.5^\circ$, then $n = (180^\circ - M_\phi)/90^\circ = 1.25$. The open loop transfer function can be expressed as shown in Eq. 52:

$$\beta(s) = \beta_0 \left(\frac{\omega_l}{s} \right)^2 \frac{(1 + s/\omega_l)^{0.75}}{(1 + s/\omega_h)^{0.25}}. \quad (52)$$

Thus, the controller transfer function would be as follow:

$$C_F(s) = C_0 \left(\frac{\omega_l}{s} \right) \frac{(1 + s/\omega_l)^{0.75}}{(1 + s/\omega_L)^{0.5}} \frac{1}{(1 + s/\omega_h)^{0.25}}. \quad (53)$$

As for the first example, if we choose $\omega_l = \omega_L$, the form of $C_F(s)$ will be similar to the first generation CRONE controller as it appears in Eq. (54)

$$C_F(s) = C_0 \left(\frac{\omega_l}{s} \right) \left(\frac{1 + s/\omega_l}{1 + s/\omega_h} \right)^{0.25}. \quad (54)$$

Example 6: Phase Margin $M_\phi = 90^\circ$

If $M_\phi = 90^\circ$, then $n = (180^\circ - M_\phi)/90^\circ = 1$. The open loop transfer function can be expressed as shown in Eq. (55):

$$C_F(s) = C_0 \left(\frac{\omega_l}{s} \right) \left(\frac{1 + s/\omega_l}{1 + s/\omega_h} \right)^{0.5}. \quad (55)$$

Hence, the controller $C_F(s)$ transfer function would be:

$$C_F(s) = C_0 \left(\frac{\omega_l}{s} \right) \frac{(1 + s/\omega_l)}{(1 + s/\omega_L)^{0.5}} \frac{1}{(1 + s/\omega_h)^{0.5}}. \quad (56)$$

As the two previous cases, when choosing $\omega_l = \omega_L$, the form of $C_F(s)$ of the second generation will be similar to the first generation CRONE controller as presented in relation (57):

$$C_F(s) = C_0 \left(\frac{\omega_l}{s} \right) \left(\frac{1 + s/\omega_l}{1 + s/\omega_h} \right)^{0.5}. \quad (57)$$

Performances

In this last section, the study will be divided into two parts referring to value of x .

For $x = 0$

To sum up, for the three cases studied regarding the value of the phase margin ($M_\phi = 45^\circ, 67.5^\circ$ and 90°), the form of the synthesized controller when using the first generation and the second generation CRONE controllers is the same. Thus, the transfer function of this controller is the same for examples 1 and 4.

However, some small differences exist between examples 5 and 6 on one hand and examples 2 and 3 on the other hand because of the choice of $\omega_l = \omega_L$. This assumption leads to $\omega_l = 0.97 \cdot 10^{-4}$ rad/s (nominal case for the Aluminum for $L = 1$ m). In fact, in the open loop, this difference can be expressed by the absence of an asymptotical behavior around the phase -135° over the interval $[10^{-4}$ rad/s; 10^{-2} rad/s] as it was the case for examples 2 and 3.

Nevertheless, for the low frequencies ($\omega < 10^{-4}$ rad/s), around the open-loop gain crossover frequency $\omega_u = 1$ rad/s and at high frequencies, the open loop behavior is identical when comparing examples 2 and 5 or examples 3 and 6. This can explain the fact that the closed loop dynamics are similar for both CRONE generations.

For $X > 0$

It is important to analyze the sensitivity of the stability degree at position of x through the phase margin a posteriori when controlling the temperature $T(0, t)$ for $x = 0$ and studying the influence of the temperature sensor when this latter is not placed at $x = 0$ exactly.

Hence, for $x > 0$, the open loop transfer function $\beta(s, x)$ can be expressed as follow:

$$\beta(s, x) = C(s)P_{2.1}(s) e^{-\left(\frac{s}{\omega_x}\right)^{0.5}}, \quad (58)$$

which can be simplified when introduction the nominal open loop transfer function $\beta_{nom}(s)$,

$$\beta(s, x) = \beta_{nom}(s) e^{-\left(\frac{s}{\omega_x}\right)^{0.5}}, \quad (59)$$

whose frequency response $\beta(j\omega, x)$ is of the following form

$$\beta(j\omega, x) = \beta_{nom}(j\omega) e^{-\left(\frac{j\omega}{\omega_x}\right)^{0.5}}. \quad (60)$$

Knowing that

$$e^{-\left(\frac{j\omega}{\omega_x}\right)^{0.5}} = m(x, \omega) e^{-j\theta(x, \omega)} \quad \text{where} \quad \begin{cases} m(x, \omega) = e^{-\left(\frac{\omega}{2\omega_x}\right)^{0.5}} = e^{-x\left(\frac{\omega}{2\alpha_d}\right)^{0.5}} \\ \theta(x, \omega) = -\left(\frac{\omega}{2\omega_x}\right)^{0.5} = -x\left(\frac{\omega}{2\alpha_d}\right)^{0.5} \end{cases} \quad (61)$$

the open loop gain and phase can be expressed as follow:

$$\begin{cases} |\beta(j\omega, x)| = |\beta_{nom}(j\omega)| m(x, \omega) \\ \arg \beta(j\omega, x) = \arg \beta_{nom}(j\omega) + \theta(x, \omega) \end{cases} \quad (62)$$

The expression of the phase margin $M_\Phi(x)$ at the gain crossover frequency, ω_u , can be represented as follow:

$$\begin{aligned} M_\Phi(x) &= \pi + \arg \beta(x, j\omega_u) \\ &= \pi + \arg \beta_{nom}(j\omega_u) + \theta(x, \omega_u) \\ &= \left(\pi - n \frac{\pi}{2}\right) - \sqrt{\frac{\omega_u}{2\alpha_d}} x. \end{aligned} \quad (63)$$

Referring to Eq. (63), one can conclude the following:

- Concerning well defined values of n , ω_u and α_d , $M_\Phi(x)$ is a decreasing linear function depending on x ;
- The negative slope is proportional to ω_u and inversely proportional to the thermal diffusivity of the material α_d ;
- The value of the order n selected based on the phase margin value does not affect the slope; thus, it does not alter the sensitivity of the stability degree of the controller for position x .

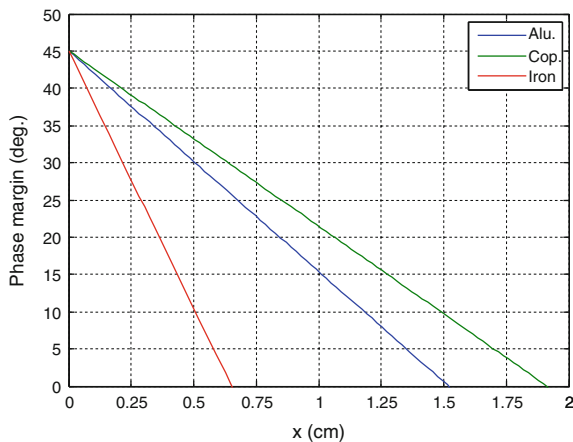
However, a special sensor placement, noted x_{crit} , allows to get a null phase margin (which yields to an oscillatory system on closed loop). Above this value, the system becomes unstable. Thus, the value x_{crit} is the following:

$$M_\Phi(x) = 0 \quad \Rightarrow \quad x_{crit} = \left(\pi - n \frac{\pi}{2}\right) \sqrt{\frac{2\alpha_d}{\omega_u}}. \quad (64)$$

When x varies between 0 and x_{crit} , another particular position exists. It will be known as the *limit position*, x_{lim} , which corresponds to a minimal phase margin, $M_{\Phi min}$, that will be set depending on the user specifications as shown in Eq. (65):

$$x_{lim} = \sqrt{\frac{2\alpha_d}{\omega_u}} \left(\pi - n \frac{\pi}{2} - M_{\Phi min}\right) \in [0; x_{crit}]. \quad (65)$$

Fig. 9 Phase margin variation $M_\phi(x)$ for $n = 1.5$ with respect to the position x (in cm) and of the used material



Thus, Fig. 9 shows the variation of the position x for the three materials when the phase margin $M_\phi(x)$ varies between 45° and 0° . For this example, the critical values are: 0.65 cm for the iron, 1.52 cm for the aluminum and 1.91 cm for the copper. Another example resides by the determination of the phase margin when x is equal to 0.5 cm: for the iron, $M_\phi = 10.5^\circ$, for the aluminum, $M_\phi = 30.2^\circ$ and $M_\phi = 33.2^\circ$ for the copper.

As an example, two simulations were realized when using the controller obtained through example 4 ($M_\phi(0) = 45^\circ$). In the first simulation (Fig. 10a), the feedback is realized based on the temperature value $T(t,0)$ measured at $x = 0$ cm. The temperature variation $T(t,0)$ at $x = 0$ and $T(t,x)$ at $x = 5$ mm are shown in Fig. 10a, c, e). In the second simulation (Fig. 10b), the feedback is realized using temperature value $T(t,x)$ measured at $x = 5$ mm. The temperature variation $T(t,0)$ at $x = 0$ and $T(t,x)$ at $x = 5$ mm are shown in Fig. 10b, d, f. Through this second case study, the influence of the sensor position uncertainties (by a value of 5 mm) is shown clearly.

Thus, Fig. 11 shows the responses for the temperature $T(t,0)$ at $x = 0$ (figures a et b), $T(t,x)$ at $x = 5$ mm (figures c et d) at the corresponding control signal $u(t)$

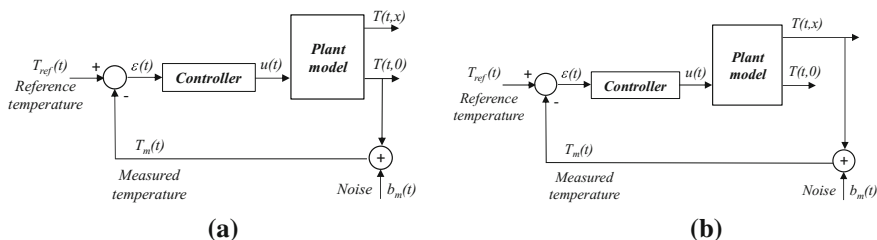


Fig. 10 Control blocks of the two study cases based on the synthesized controller of example 4 ($M_\phi(0) = 45^\circ$): **a** feedback realized based on the temperature at $x = 0$; **b** feedback realized based on the temperature at $x = 5$ mm

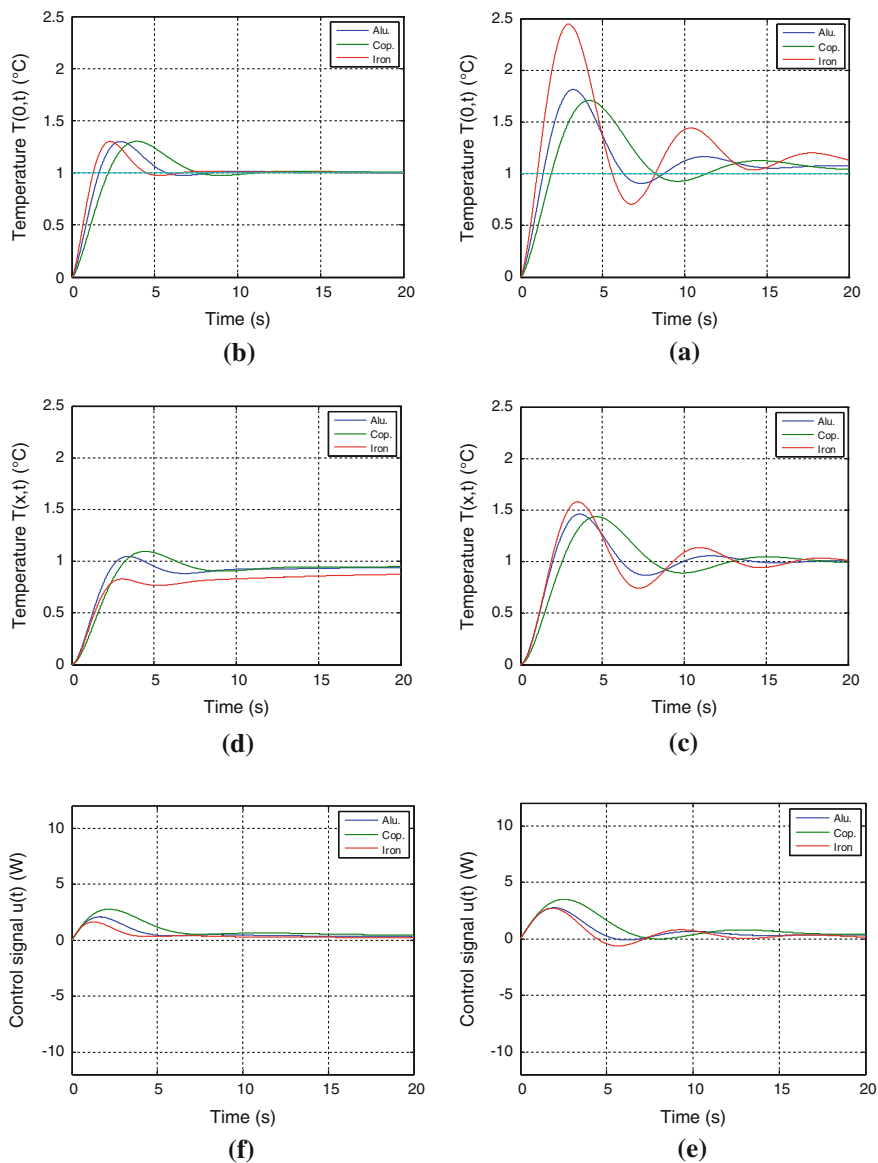


Fig. 11 Temperature response of $T(t,0)$ at $x = 0$ (1st line: **a**, **b** $T(t,x)$ at $x = 5$ mm (2nd line: **c**, **d**) and for the control signal $u(t)$ (3rd line: **e**, **f**) for a step input of 1 $^{\circ}\text{C}$ for the aluminum, the copper and the iron, when considering a feedback control based on the temperature at $x = 0$ (figures **a**, **c**, **e**) and for a temperature measured at $x = 5$ mm (figures: **b**, **d**, **f**)

(figures e et f) for a step input of 1 °C for the aluminum, the copper and the iron when considering a feedback control based on the temperature at $x = 0$ (figures a, c et e) and for a temperature measured at $x = 5$ mm (figures: b, d et f). Based on these figures, one can conclude the following:

When the **positioning sensor uncertainties are absent at $x = 0$ mm**, the robustness of the stability degree is confirmed (Fig. 11a). Thus, the three step responses are almost equal. So, when comparing them with the nominal response obtained for the aluminum, the two other responses would be expressed as a dilatation (for the copper) or a contraction (for the iron) concerning the time domain axis. However, when $x > 0$ mm, this property is no more conserved (referring to the simulation where the sensor is positioned at 5 mm—Fig. 11c).

However, when the **positioning uncertainties are present at $x = 5$ mm**, the robustness of the stability degree is no more conserved whatever the material in use is and for any positioning of the temperature sensor (for $x = 0$, Fig. 11b). This result is logic as the variation of x affects the phase margin as already presented in Fig. 8.

A particular attention should be point out on the control signal $u(t)$ whose value remains below the saturation limit ($U_{max} = 12$ W).

4 Conclusions

In this chapter, we have introduced first the general transfer function of a finite diffusive interface medium in order to study the heat diffusion across its central axis. The study is conducted over three different materials (Iron, Copper and Aluminum) to study the robustness of the controller.

The CRONE controller was the one used in this study. The first two generations were applied. The controller of the first generation is calculated a priori where the phase is constant over all the frequency bandwidth whereas the second generation is deduced using the loop shaping and it applies whenever the phase is constant with gain variations for the plant.

Two scenarios were proposed: the first one shows a gain variation with a constant phase and both CRONE generations were applied. All results were almost similar. For the second scenario, the plant's gain was varying while the phase was maintained constant around ω_u which yield in the use of the second CRONE generation.

Concerning the future works, lot of adjustments could be made to enrich this work. First, some new scenarios could be proposed in order to analyze the behavior of the third generation CRONE controllers and to compare this controller to other ones. Added to that, the implementation of some observers could be interesting as we will not be able to measure the temperature at any point of the bar due to some physical/technical limitations. The last and most interesting point is to implement physically this system and to be able to compare the real measurements to the simulated ones. Whenever the test bench is realized, the identification of the

equation that would model this system will be made and a comparison between the real one and the approximated one will be proposed. Then, the control of this plant using the LabView software along with the data acquisition board will be performed. The performance analysis of the observers will be a novel study applied in a fractional order environment.

References

1. Abi Zeid Daou, R., & Moreau, X. (2015). *Fractional calculus: Applications*. New York: Nova.
2. Abi Zeid Daou, R., Moreau, X., Assaf, R., & Christohpy, F. (2012). Analysis of HTE fractional order system in the thermal diffusive interface—part 1: Application to a semi-infinite plane medium. In *International Conference on Advances in Computational Tools for Engineering Applications*, Lebanon.
3. Assaf, R., Moreau, X., Abi Zeid Daou, R., & Christohpy, F. (2012). Analysis of HTE fractional order system in HTE thermal diffusive interface—part 2: Application to a finite medium. In *International Conference on Advances in Computational Tools for Engineering Applications*, Lebanon.
4. Azar, A. T., & Serrano, F. (2014). Robust IMC-PID tuning for cascade control systems with gain and phase margin specifications. *Neural Computing and Applications*, 25(5).
5. Azar, A. T., & Serrano, F. (2015). Design and modeling of anti wind up PID controllers. *Complex System Modelling and Control Through Intelligent Soft Computations*, 319.
6. Azar, A. T., & Zhu, Q. (2015). Advances and applications in sliding mode control systems. Study in computational intelligence (Vol. 576). Springer.
7. Battaglia, J., Cois, O., Puigsegur, L., & Oustaloup, A. (2001). Solving an inverse heat conduction problem using a non-integer identified model. *International Journal of Heat and Mass Transfer*, 44(14), 2671–2680.
8. Boulkroune, A., Bouzeriba, A., Bouden, T., & Azar, A. T. (2016). *Fuzzy adaptative synchronization of uncertain fractional-order chaotic systems*. Control: Advances in Chaos Theory and Intelligent. 337.
9. Charef, A., & Fergani, N. (2010). PI λ D μ controller tuning for desired closed-loop response using impulse response. In *Workshop on Fractional Derivation and Applications*, Spain.
10. Cois, O. (2002). *Systèmes linéaires non entiers et identification par modèle non entier: application en thermique*. Bordeaux: Université Bordeaux I.
11. CRONE Group. (2005). *CRONE control design module*. Bordeaux: Bordeaux University.
12. Lin, J. (2001). *Modélisation et identification de systèmes d'ordre non entier*. Poitiers: Université de Poitiers.
13. Magin, R., Ortigueira, M., Podlubny, I., & Trujillo, J. (2011). On the fractional signals and systems. *Signal Processing*, 91(3), 350–371.
14. Malti, R., Sabatier, J., & Akçay, H. (2009). Thermal modeling and identification of an aluminium rod using fractional calculus. In *15th IFAC Symposium on System Identification*, France.
15. Miller, K., & Ross, B. (1993). *An introduction to the fractional calculus and fractional differential equations*. New York: Wiley.
16. Oldham, K., & Spanier, J. (1974). *The fractional calculus*. New York: Academic Press.
17. Oustaloup, A. (1975). *Etude et Réalisation d'un système d'asservissement d'ordre 3/2 de la fréquence d'un laser à colorant continu*. Bordeaux: Universitu of Bordeaux.

18. Poinot, T., & Trigeassou, J. (2004). Identification of fractional systems using an output-error technique. *Nonlinear Dynamics*, 38(1), 133–154.
19. Trigeassou, J.-C., Poinot, T., Lin, J., Oustaloup, A., & Levron, F. (1999). Modeling and identification of a non integer order system. In *European Control Conference*. Karlsruhe: IFAC.

Fractional Order Control and Synchronization of Chaotic Systems

Azar, A.T.; Vaidyanathan, S.; Ouannas, A. (Eds.)

2017, XII, 877 p. 468 illus., 175 illus. in color.,

Hardcover

ISBN: 978-3-319-50248-9